



# CHORUS

This is the accepted manuscript made available via CHORUS. The article has been published as:

Superconductivity and topological properties of  $\text{MgB}_2$ -type diborides from first principles

Yipeng An, Jie Li, Kun Wang, Guangtao Wang, Shijing Gong, Chunlan Ma, Tianxing Wang, Zhaoyong Jiao, Xiao Dong, Guoliang Xu, Ruqian Wu, and Wuming Liu

Phys. Rev. B **104**, 134510 — Published 14 October 2021

DOI: [10.1103/PhysRevB.104.134510](https://doi.org/10.1103/PhysRevB.104.134510)

# Superconductivities and topological properties of MgB<sub>2</sub>-type diborides from first-principles

Yipeng An,<sup>1,\*</sup> Jie Li,<sup>2</sup> Kun Wang,<sup>3,4</sup> Guangtao Wang,<sup>1</sup> Shijing Gong,<sup>5</sup> Chunlan Ma,<sup>6</sup> Tianxing Wang,<sup>1</sup> Zhaoyong Jiao,<sup>1</sup> Xiao Dong,<sup>1</sup> Guoliang Xu,<sup>1</sup> Ruqian Wu,<sup>2,†</sup> and Wuming Liu<sup>7,‡</sup>

<sup>1</sup>*School of Physics, Henan Normal University, Xinxiang 453007, China*

<sup>2</sup>*Department of Physics and Astronomy, University of California, Irvine 92697, USA*

<sup>3</sup>*Department of Physics and Astronomy, Mississippi State University, Mississippi State 39762, USA*

<sup>4</sup>*Department of Chemistry, Mississippi State University, Mississippi State 39762, USA*

<sup>5</sup>*Key Laboratory of Polar Materials and Devices (MOE) & Department of Optoelectronics, East China Normal University, Shanghai 200062, China*

<sup>6</sup>*School of Physics and Technology, Suzhou University of Science and Technology, Suzhou 215009, China*

<sup>7</sup>*Beijing National Laboratory for Condensed Matter Physics, Institute of Physics, Chinese Academy of Sciences, Beijing 100190, China*

The superconductivities and topological properties of MgB<sub>2</sub>-type diborides are investigated by means of the first-principles calculations with different exchange-correlation functionals. Functionals with the van der Waals (vdW) correction (such as OptB88-vdW) may predict critical temperature ( $T_c$ ) comparable to experimental results for several MgB<sub>2</sub>-type superconductors, particularly for the pristine MgB<sub>2</sub> (39.3 K versus 39 K). Interestingly, the spin-fluctuation (SF) is found to play a significant role for the superconducting behavior of diborides with transition metal elements and their  $T_c$  can be enhanced monotonically by applying tensile strains. Furthermore, Dirac surface states of TaB<sub>2</sub> and NbB<sub>2</sub> are revealed, suggesting their potential use as topological superconducting materials. This work provides a

---

\* ypan@htu.edu.cn; † wur@uci.edu; ‡ wmliu@iphy.ac.cn

useful guideline for *ab initio* studies of superconductivities and topological properties of vdW layered materials.

## I. INTRODUCTION

To search and design superconductors for applications, one of the sensible strategies is predicting their critical temperature ( $T_c$ ) from ground state properties at zero temperature with a dependable theoretical framework. Although it remains a challenge to achieve this goal for general superconducting materials, a few successful theories have been developed in the last half century, and the seminal theory of Bardeen, Cooper, and Schrieffer (BCS) was the outstanding example [1]. In principle, the anisotropic Migdal-Eliashberg (ME) approach [2,3] can provide reliable quantitative determination of anisotropic temperature-dependent superconducting gap ( $\Delta$ ) and  $T_c$  of conventional superconductors that rely on phonon-mediated interaction between electrons. The computational cost can be further reduced by combining with electron-phonon coupling (EPC) interpolation based on maximally localized Wannier functions [4-7]. Empirical models such as the Morel-Anderson theory [8] and McMillan's formula [9-11] using adjustable parameters may also give  $T_c$  of conventional isotropic superconductors close to the solution of Eliashberg equations [12].

In recent years, the application of density functional theory (DFT) for studies of superconductors (SCDFT) was proved to be powerful in predicting new superconducting materials without the need of empirical parameters [13-15] as well as in explaining the physical mechanisms of superconductivity [16-19], especially for cases under a pressure [20]. A great deal of effort has been dedicated to further empower the predictability of the SCDFT

scheme by examining or developing appropriate exchange-correlation functionals [18], considering the anisotropic natures of electron-phonon coupling, or including plasmons [21], spin-fluctuation [22], and the spin-orbit interaction [23]. Particularly, as the complexities of many-body interactions are mostly invoked in the exchange and correlation term, the applicability of different functionals for the studies of superconductivity has not been carefully examined and poor results were occasionally obtained. For instance,  $T_c$  of a prototypical anisotropic superconductors  $\text{MgB}_2$  was reported to be only 22 K [24] via DFT calculations with the generalized gradient approximation (GGA) [25] and ultrasoft pseudopotentials [26], far smaller than its experiment value of 39 K [27]. This value was increased to 35.4 K by using a newly developed functional [18], showing a large room for getting accurate description of superconductivities with *ab initio* theory.

In this paper, we study the superconductivities of several  $\text{MgB}_2$ -type diborides with the vdW layered structure, namely,  $\text{MgB}_2$ , and VB-group diborides  $\text{MB}_2$  ( $M = \text{V}, \text{Nb}, \text{Ta}$ ), by means of first-principles calculations. We evaluate different exchange-correlation functionals, from the conventional Perdew-Burke-Ernzerhof (PBE) functional [25,28], revPBE [29], PBEsol [30], to those with the vdW correction, such as OptB88-vdW (OPT) [31-33], which has been widely used for the structural optimization of vdW layered materials [34,35]. Our results unveil that the OPT functional can provide excellent results of superconductivities of  $\text{MgB}_2$ -type vdW layered structures, including giving the best theoretical  $T_c = 39.3$  K of  $\text{MgB}_2$  to date. Our other key results include 1) a reasonable stretch strain may lead to monotonical increase of  $T_c$ ; 2) the spin-fluctuation plays a significant role in determining the superconductivities of VB-group diborides; 3) the  $\text{TaB}_2$  and  $\text{NbB}_2$  show the time-reversal symmetry protected topological Dirac surface states in their spectral function. These findings open a new vista for exploring emergent properties of superconducting and topological materials and, more importantly, for integrating them in potential applications.

## II. COMPUTATIONAL DETAILS

According to the SCDFT, the critical superconducting gap at a wave-vector  $\mathbf{k}$  is described as

$$\Delta_{n\mathbf{k}} = -\frac{1}{2} \sum_{n'\mathbf{k}'} \frac{K_{nkn'\mathbf{k}'}(\xi_{n\mathbf{k}}, \xi_{n'\mathbf{k}'})}{1 + Z_{n\mathbf{k}}(\xi_{n\mathbf{k}})} \times \frac{\Delta_{n'\mathbf{k}'}}{\sqrt{\xi_{n'\mathbf{k}'}^2 + \Delta_{n'\mathbf{k}'}}^2} \tanh\left(\frac{\sqrt{\xi_{n'\mathbf{k}'}^2 + \Delta_{n'\mathbf{k}'}}^2}{2T}\right), \quad (1)$$

where  $\xi_{n\mathbf{k}}$  is the  $n$ th eigenvalue of normal-state Kohn-Sham (KS) orbital measured from the Fermi level ( $E_F$ ).  $K_{nkn'\mathbf{k}'}(\xi, \xi')$  refers to the superconducting-pair creation and annihilation interactions with following three terms:

$$K_{nkn'\mathbf{k}'}(\xi, \xi') \equiv K_{nkn'\mathbf{k}'}^{ee}(\xi, \xi') + K_{nkn'\mathbf{k}'}^{ep}(\xi, \xi') + K_{nkn'\mathbf{k}'}^{sf}(\xi, \xi'), \quad (2)$$

namely, the electron-electron Coulomb repulsion, the electron-phonon coupling, and the alternative spin-fluctuation kernel. The electron-phonon renormalization factor  $Z_{n\mathbf{k}}(\xi)$  is comprised of the EPC and alternative SF terms as

$$Z_{n\mathbf{k}}(\xi) = Z_{n\mathbf{k}}^{ep}(\xi) + Z_{n\mathbf{k}}^{sf}(\xi), \quad (3)$$

as the contribution from the Coulomb repulsion is already included in the KS eigenvalue  $\xi_{n\mathbf{k}}$ .

$T$  is the temperature defined by considering the Boltzmann constant  $k_B = 1$ . More details about the forms of  $K$  and  $Z$  used in this work can be found in previous reports [14,19]. Note that a recently proposed functional of  $K$  and  $Z$  sets a new standard for the balance of accuracy and computational cost in simulating the superconductivity [18]. The  $T_c$  is obtained using the bisection method [19], with the initial lower limit  $T_c^{\min}$  being set to zero, and the initial upper limit  $T_c^{\max}$  being set according to the BCS theory ( $2\Delta_0/3.54$ , where  $\Delta_0$  refers to the superconducting gap averaged over Fermi surfaces at 0 K, this value is doubled if there is a finite gap at this temperature). The gap equation 1 is solved at  $T = (T_c^{\min} + T_c^{\max})/2$  and, either  $T_c^{\max}$  or  $T_c^{\min}$  is replaced by  $T$  in the following steps based on whether the amplitude of average gap is small enough (i.e.,  $\langle |\Delta| \rangle < 10^{-3} \Delta_0$ ). The procedure repeats ten times, and  $T_c$  is

obtained as the average of  $T_c^{\min}$  and  $T_c^{\max}$ , which are very close to each other.

In this work, the first-principles self-consistent and electron-phonon coupling calculations are performed with the Quantum ESPRESSO (QE) code [36]. The SG15 optimized Norm-Conserving Vanderbilt (ONCV) pseudopotentials [37-39] are employed to describe the effect of core electrons. The plane-wave kinetic-energy cutoff and the energy cutoff for charge density are set to 80 and 320 Ry, respectively. Different exchange-correlation functionals are assessed [25,28-33]. The Brillouin-zone integrations are calculated by the optimized tetrahedron method [40] using a  $12 \times 12 \times 12$  grid. A denser grid ( $24 \times 24 \times 24$ ) is used to obtain the density of states and band structures, while coarse grid ( $6 \times 6 \times 6$ ) is adopted for the phonon calculations. The total energy tolerance and residual force on each atom are less than  $10^{-8}$  Ry and  $10^{-6}$  Ry Bohr<sup>-1</sup> in the geometry optimization. The phonon frequencies and electron-phonon vertices are obtained using the density functional perturbation theory (DFPT) [41]. The SCDFT calculations are performed using the Superconducting-Toolkit (SCTK) [17,42]. The normal state of electronic structure is read from the self-consistent results of QE with the same  $k$ -points mesh. The electron-phonon coupling and kernel term of Eq. 2 are obtained with the same grid of  $k$ -points as in the phonon calculations.

The work function ( $\Phi$ ) and spectral function of surface structures are obtained by the surface Green's function method as implemented in the QuantumATK (ATK) [43-45]. Linear combinations of atomic orbitals (LCAO) are employed to expand the wave functions of valence states. The SG15 ONCV pseudopotentials [37-39], GGA-PBE functional [25,28], and Grimme's DFT-D2 [46] vdW correction are used. A real-space grid density that is equivalent to a plane-wave kinetic energy cutoff of 60 Ha is adopted. A  $12 \times 12 \times 300$  Monkhorst-Pack  $k$ -points mesh is set for the Brillouin zone sampling of the surface structures. The topological

indices [47,48] are obtained from a post-processing procedure of the self-consistent calculations by ATK including the spin-orbital coupling interactions.

### III. RESULTS AND DISCUSSION

Extensive efforts [4,18,49,50] have been made to theoretically reproduce the experimental  $T_c$  of anisotropic superconductor such as MgB<sub>2</sub> [27]. The best  $T_c$  of MgB<sub>2</sub> obtained from SCDFT calculations was recently reported to be 35.4 K, based on the new functionals of electron-phonon superconducting-pair interactions and electron-phonon renormalization factor [18]. This result is rather close to the experimental value [27]. As a benchmark, we re-evaluate the superconductivities of MgB<sub>2</sub> again by using different exchange-correlation functionals from PBE [25,28], revPBE [29], and PBEsol [30], to OptB88-vdW [31-33]. The OPT functional includes the vdW dispersion force, which is essential to provide accurate predictions for structures of vdW layered materials [34,35,51].

TABLE I. Superconducting parameters of MgB<sub>2</sub> with experimental structure<sup>a</sup> obtained with different functionals.

	PBE	revPBE	PBEsol	OptB88-vdW
$T_c$ (K) <sup>b</sup>	23.4	24.0	19.3	39.3
$T_{c-SF}$ (K)	18.1	18.7	14.4	33.2
$Z_{ave}$	0.61	0.61	0.58	0.76
$\Delta_{max}$ (meV)	5.99	6.02	5.22	9.63
$\Delta_{min}$ (meV)	0.85	0.84	0.76	1.18
$\lambda_{ave}$	0.65	0.64	0.61	0.80
$\mu_{ave}^*$	0.28	0.28	0.28	0.28

<sup>a</sup>The experimental structure with lattice  $a$  ( $c$ )=3.086 (3.524) Å [27]; <sup>b</sup>The experimental  $T_c$  is 39 K [27], and other theoretical  $T_c$ 's are 35.4 K [18], 34.1 K [50], and 49 K [4], respectively.

Several key superconducting parameters of MgB<sub>2</sub> with either the experimental structure [27] or the optimized structure obtained with these functionals are shown in Table I and Table SI in the Supplemental Material (SM) [52], respectively. Noticeably, the calculated  $T_c$  of MgB<sub>2</sub> is 39.3 K with OptB88-vdW functional, in excellent agreement with the experimental value (39 K) [27]. It is worth noting that this is the best theoretical  $T_c$  of MgB<sub>2</sub> so far. In

contrast, the PBE-based functionals seriously underestimate the  $T_c$  of MgB<sub>2</sub> for both cases without ( $T_c$ ) and with ( $T_{c-SF}$ ) SF.

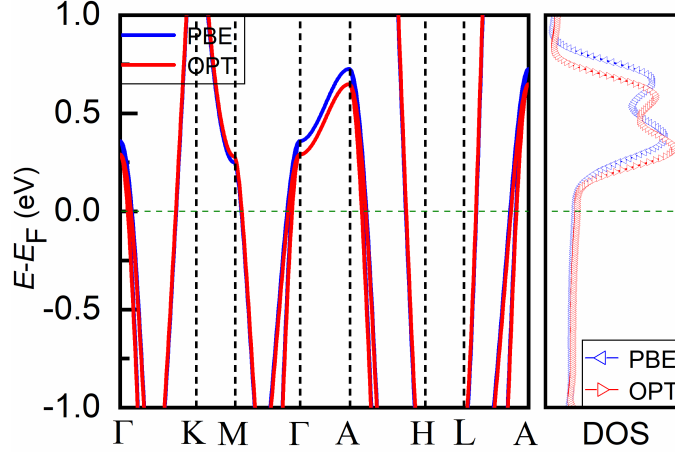


FIG. 1. Band structures and density of states (DOSs) of MgB<sub>2</sub> obtained with PBE and OptB88-vdW (OPT) functionals, respectively. The  $E_F$  is shifted to zero.

The present results strongly suggest that the inclusion of vdW correction is crucial in studies of MgB<sub>2</sub>-type superconductors. This can be attributed to the fact that the OPT functional makes slight downward shift of bands (see Fig. 1) and increases the density of states (DOSs) at the Fermi level ( $D_0$ ). The electron-phonon coupling constant  $\lambda$  (i.e.,  $\lambda_{qv}$  and  $\lambda_{nk}$ ) thus increases (see Fig. 2) since it is proportional to  $D_0$  [9]. The EPC is very strong near the  $\Gamma$  point and along the  $\Gamma$ -A path. The phonons obtained using the OPT functional are overall softened, especially for the bond-stretching mode (i.e., the  $E_{2g}$  mode) along the  $\Gamma$ -A path [53]. A large  $\lambda$  is observed due to the contributions of long-range interactions. The OPT functional appears to be more accurate in describing the electron-phonon interactions of MgB<sub>2</sub>. It gives a larger electron-phonon renormalization factor  $Z_{ave}$  (average over the Fermi surface) than those from PBE functionals. This results in wider superconducting gaps whose maximum ( $\Delta_{max}$ ) and minimum ( $\Delta_{min}$ ) values are 9.63 and 1.18 meV, respectively (see Table I).

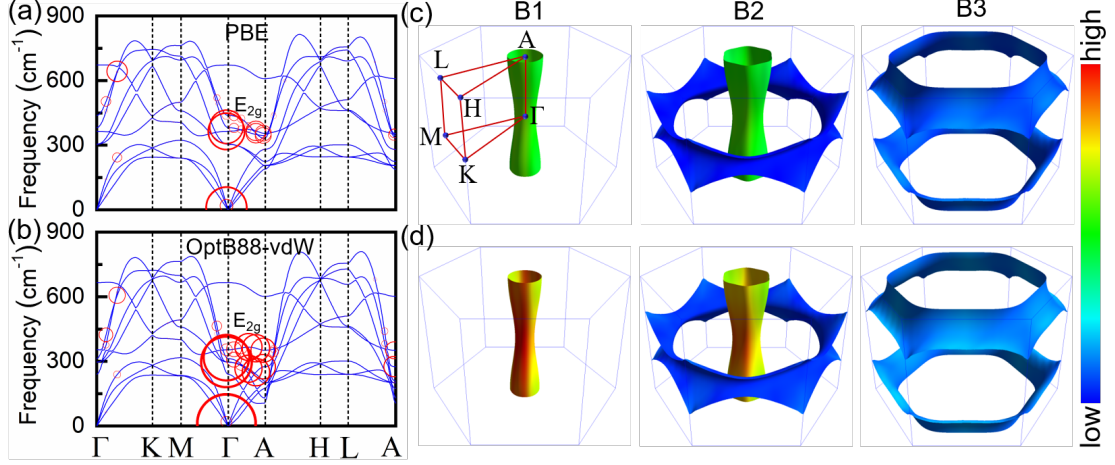


FIG. 2. Phonon band structures, electron-phonon coupling constants  $\lambda_{q\nu}$ , and  $\lambda_{nk}$  on Fermi surfaces. (a) and (c) for PBE, (b) and (d) for OptB88-vdW functional, respectively. The red radii of circles in (a) and (b) indicate magnitude of electron-phonon coupling constant  $\lambda_{q\nu}$  at wave-vector  $\mathbf{q}$  and branch  $\nu$ . B1, B2, and B3 refer to the three bands crossing the Fermi level. Fermi surfaces are drawn by using the FermiSurfer code [54]. (c) and (d) have the same color scales. The first Brillouin zone of  $\text{MgB}_2$  bulk is shown in B1 of (c).

The Coulomb pseudopotential  $\mu_{\text{ave}}^*$  (average over the Fermi surface), which is usually treated as an adjustable parameter for the conventional Allen-Dynes-modified McMillan formula [9-11],

$$T_c = \frac{\omega_{\text{ln}}}{1.2} \exp \left[ \frac{-1.04(1 + \lambda)}{\lambda - \mu^*(1 + 0.62\lambda)} \right], \quad (4)$$

can be obtained via converse calculations of EPC constant  $\lambda$  and averaged phonon frequencies  $\omega_{\text{ln}}$ , namely,

$$\lambda = \sum_{q\nu} \lambda_{q\nu}, \quad (5)$$

$$\lambda_{q\nu} = \frac{2}{D_0 \omega_{q\nu}} \sum_{knn'} |g_{nk n'k+q}^\nu|^2 \delta(\xi_{nk}) \delta(\xi_{n'k+q}), \quad (6)$$

$$\omega_{\text{ln}} = \exp \left[ \frac{1}{\lambda} \sum_{q\nu} \lambda_{q\nu} \ln(\omega_{q\nu}) \right], \quad (7)$$

where  $\lambda_{q\nu}$  and  $\omega_{q\nu}$  refer to the EPC constant and phonon frequency at wave-vector  $\mathbf{q}$  and

branch  $\nu$ , respectively.  $D_0$  is the DOS at the  $E_F$ , and  $g$  is the electron-phonon matrix element [41]. The Brillouin-zone integrals are calculated using the optimized tetrahedron method [40] with a dense  $\mathbf{k}$  grid. Although the EPC constant  $\lambda_{\text{ave}}$  (average over the Fermi surface) obtained with the OPT functional is the highest, these functionals produce the same Coulomb pseudopotential ( $\mu_{\text{ave}}^* = 0.28$ ) that is much larger than the empirical value  $0.10 \sim 0.16$  [11].

TABLE II. Superconducting parameters of MgB<sub>2</sub> under different stretch strains (negative pressure).

Stretch strains (Kbar)	$a$ (Å)	$c$ (Å)	$T_c$ (K)	$Z_{\text{ave}}$	$\Delta_{\text{max}}$ (meV)	$\Delta_{\text{min}}$ (meV)	$\lambda_{\text{ave}}$	$\mu_{\text{ave}}^*$
0	3.034	3.470	29.4	0.64	7.08	0.91	0.68	0.28
50	3.062	3.538	35.6	0.72	8.71	1.06	0.77	0.28
75	3.079	3.577	40.3	0.79	9.83	1.23	0.83	0.28
100	3.096	3.621	45.1	0.87	11.20	1.34	0.92	0.28
110	3.104	3.640	48.9	0.91	11.86	1.44	0.96	0.28
125 (unstable)	3.116	3.671	53.3	0.99	12.99	1.65	1.05	0.28

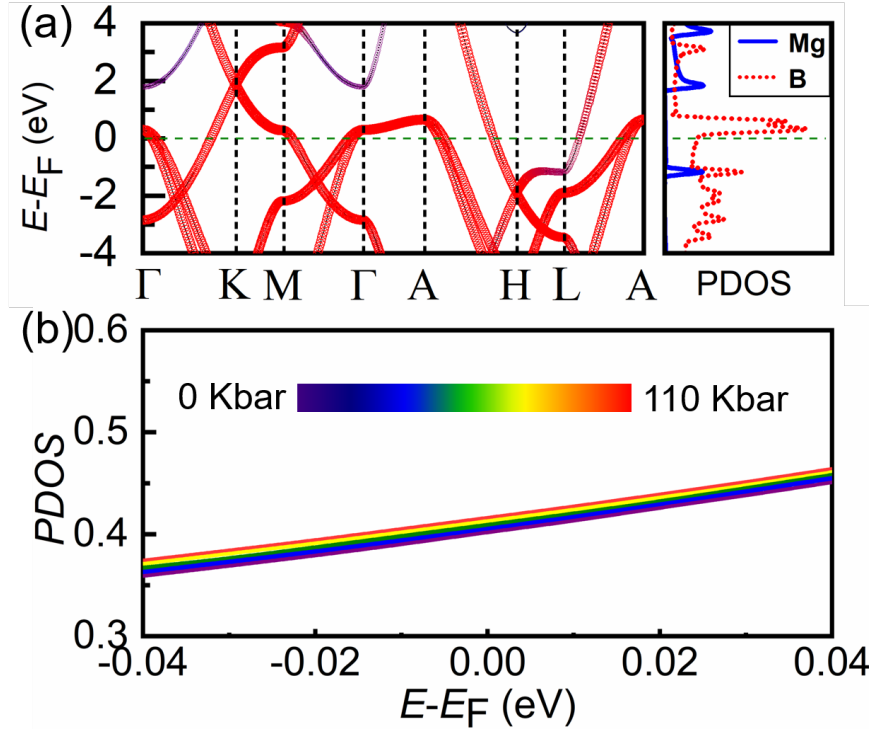


FIG. 3. (a) Projected band structures and projected density of states (PDOSs) of MgB<sub>2</sub>. (b) PDOSs of B atom of MgB<sub>2</sub> under different stretch strains.

Various methods have been attempted to increase  $T_c$  of superconductors, including

high-pressure [55,56], stretching [57], doping [58], and magic-angle [59]. Most of these methods cause structural changes (e.g., lattice parameters). Note that the optimized structures are smaller than experimental ones and indeed give much reduced  $T_c$  for all functionals (see Table SI in the SM [52]), e.g., from 39.3 to 29.4 K for the OPT functional. In contrast, lattice stretch may significantly increase  $T_c$  of MgB<sub>2</sub> to a maximum value of 48.9 K (see Table II) under a strain of 110 Kbar (i.e., negative pressure). This is due to the enhanced PDOS value of B-2p orbitals near the  $E_F$ , which dominates the superconducting behavior of MgB<sub>2</sub> (see Fig. 3). We see that the  $Z_{ave}$ ,  $\Delta_{max}$ ,  $\Delta_{min}$ , and  $\lambda_{ave}$  of MgB<sub>2</sub> increase monotonically with the stretch, but  $\mu_{ave}^*$  remains unchanged (see Table II). Note that the MgB<sub>2</sub> remains stable under a reasonable stretch ( $< 110$  Kbar). Negative frequencies appear in phonon bands as the stretch is too large (such as 125 Kar in Fig. S1 of the SM [52]). Its lattice parameters ( $a$  and  $c$ ) and  $T_c$  increase monotonically with the stretch (see Table II). Obviously, the appropriate geometry is one of the key factors for the reliable prediction of  $T_c$ . Furthermore, one may significantly enhance  $T_c$  of MgB<sub>2</sub> by applying a tensile strain.

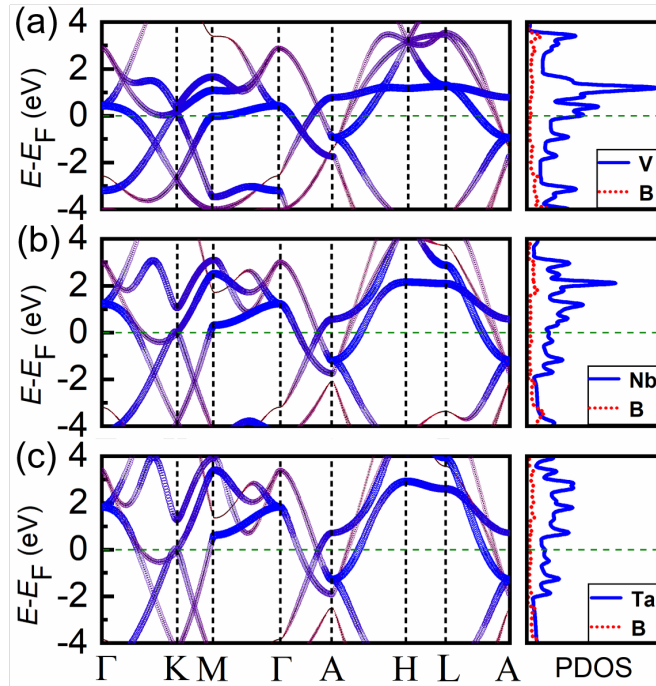


FIG. 4. Projected band structures and PDOS of VB<sub>2</sub> (a), NbB<sub>2</sub> (b), and TaB<sub>2</sub> (c). The  $E_F$  is shifted to zero.

We can now apply the same approach to study other transition metal diborides  $MB_2$  (such as  $M = V, Nb, Ta$ ). We first examine their electronic structures (see Fig. 4) and compare them with  $MgB_2$ . It can be seen that their projected band structures are significantly different from that of  $MgB_2$ , and their states around  $E_F$  are mostly from transition metal elements rather from B as in  $MgB_2$  (see Fig. 3). From results in Table III,  $VB_2$  has a very low  $T_c$  (without SF) or  $T_{c-SF}$  (with SF),  $<1$  K, in consistent with recent experiment observation [60]. Due to larger electron-phonon renormalization factor  $Z_{ave-SF}$  and superconducting gap,  $NbB_2$  and  $TaB_2$  have higher critical temperatures,  $T_{c-SF} = 7.9$  and  $12.4$  K. These values are closer to the corresponding experimental values [61-64] than those without considering SF. This demonstrates that SF plays a significant role in determining superconductivities of transition metal diborides. Note that the EPC constant  $\lambda_{ave}$  increases from  $VB_2$  to  $NbB_2$  and  $TaB_2$ , but their Coulomb pseudopotential,  $\mu_{ave-SF}^*$  (see  $\mu_{nk}$  in Fig. S3 in the SM [52]) shows a reverse trend. This is associated with the softened acoustic vibrations arising from the change of mass of transition metal atoms (see Fig. S4 in the SM [52]).

TABLE III. Lattice parameters and superconductivities of VB-group  $MB_2$  ( $M = V, Nb, Ta$ ).

	$VB_2$	$NbB_2$	$TaB_2$
$a$ (Å)	2.966	3.088	3.025
$c$ (Å)	3.005	3.305	3.254
$T_c$ (K)	0.97	10.2	13.8
$T_{c-SF}$ (K)	0.78 <sup>c</sup>	7.9 <sup>d</sup>	12.4 <sup>e</sup>
$Z_{ave-SF}$	0.47	0.70	0.95
$\Delta_{max-SF}$ (meV)	0.27	2.33	3.08
$\Delta_{min-SF}$ (meV)	-0.39	0.38	1.06
$\lambda_{ave}$	0.30	0.68	0.92
$\mu_{ave-SF}^*$	0.66	0.31	0.25

<sup>c</sup> $VB_2$  is not superconducting beyond 2K in experiment [60]; <sup>d</sup>The experimental  $T_c$ 's of  $NbB_2$  are 9 K [64], 5 K [62], and 9.4 K [61]; <sup>e</sup>The experimental  $T_c$  of  $TaB_2$  is 9.5 K [63].

To gain deeper insights into the superconducting behaviors of these diborides, we depict the Fermi velocities  $|V_F|$  of the normal electronic states, electron-phonon renormalization factor  $Z_{nk}$ , and superconducting gap  $\Delta_{nk}$  on Fermi surfaces in Fig. 5. In the first glance,  $|V_F|$ ,  $Z_{nk}$ , and  $\Delta_{nk}$  of these materials are very anisotropic. For instance, the ratio between the maximum and the minimum values of  $|V_F|$  for TaB<sub>2</sub> is as high as 213. For MgB<sub>2</sub>, there are three bands crossing  $E_F$  and its  $|V_F|$  is mostly dominated by the B-2p orbitals, especially on the cylindrical Fermi surfaces around the  $\Gamma$  point [see Fig. 5(a)]. This contributes the most of  $Z_{nk}$  [see Fig. 5(e)] and  $\Delta_{nk}$  [see Fig. 5(i)]. The Fermi surfaces of MB<sub>2</sub> appear like a “flying saucer” with a large cavity around the  $\Gamma$  point (see the top views in Fig. 5 and side views in Fig. S2 in the SM [52]). Although MB<sub>2</sub> diborides have four bands crossing  $E_F$  (except VB<sub>2</sub> which has three), the crossing points are far from the  $\Gamma$  point. Their  $|V_F|$  are typically small as these states are mostly from localized transition metal orbitals. The magnitudes of their  $|V_F|$ ,  $Z_{nk}$ , and  $\Delta_{nk}$  increase from VB<sub>2</sub> to NbB<sub>2</sub> and TaB<sub>2</sub>, leading to gradual increase of  $T_c$ .

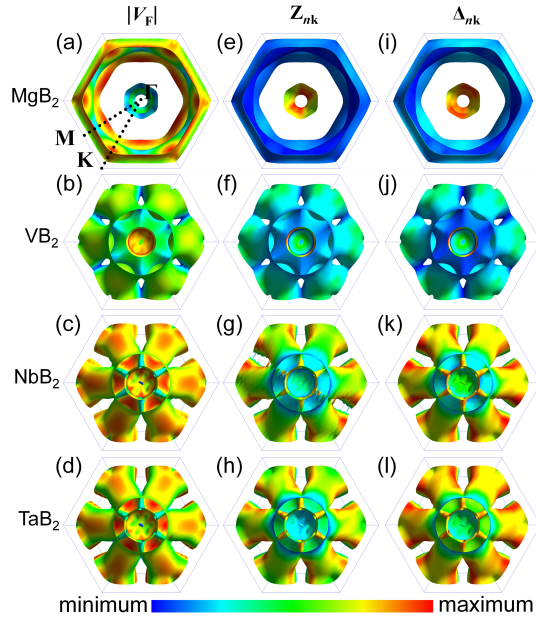


FIG. 5. Top views of Fermi velocity of the electronic states  $|V_F|$ , electron-phonon coupling renormalization  $Z_{nk}$ , and superconducting gap function  $\Delta_{nk}$  on the cylindrical and “flying saucer”-like Fermi surfaces of MgB<sub>2</sub> (a), VB<sub>2</sub> (b), NbB<sub>2</sub> (c), and TaB<sub>2</sub> (d). Their side views are shown in the Fig. S2 of the SM [52]. (a)-(d) for  $|V_F|$ , (e)-(h) for  $Z_{nk}$ , and (i)-(l) for  $\Delta_{nk}$ . The color bar indicates their minimum and maximum values.

It is found that the ratio of DOS at the  $E_F$  between B and metal atoms gradually increases from  $\text{VB}_2$  (1:6.6) to  $\text{NbB}_2$  (1:3.2) and  $\text{TaB}_2$  (1:2.5), but remains much smaller than that of  $\text{MgB}_2$  (295.7:1). As a result, their  $T_c$  follow the trend of  $T_c(\text{VB}_2) < T_c(\text{NbB}_2) < T_c(\text{TaB}_2) < T_c(\text{MgB}_2)$ . This suggests that the  $T_c$  of VB-group diborides can be further enhanced if one may increase the PDOS of B atom, such as by applying a lattice stretch that can lead to the increase of  $Z_{\text{ave-SF}}$ ,  $\Delta_{\text{max-SF}}$ ,  $\Delta_{\text{min-SF}}$ , and  $\lambda_{\text{ave}}$ . Table IV shows the results of  $\text{TaB}_2$  under different tensile strains. It can be observed that as its lattice parameters  $a$  and  $c$  increase,  $T_c$  can be enhanced to 16.1 K at a negative pressure of 150 Kbar, under which the  $\text{TaB}_2$  is still stable without any negative frequency phonon branch (see Fig. S5 in the SM [52]).

TABLE IV. Superconducting parameters of  $\text{TaB}_2$  under different stretch strains.

Stretch strains (Kbar)	$a$ (Å)	$c$ (Å)	$T_{c\text{-SF}}$ (K)	$Z_{\text{ave-SF}}$	$\Delta_{\text{max-SF}}$ (meV)	$\Delta_{\text{min-SF}}$ (meV)	$\lambda_{\text{ave}}$	$\mu_{\text{ave-SF}}^*$
0	3.025	3.254	12.4	0.95	3.08	1.06	0.92	0.25
75	3.048	3.289	13.9	1.07	3.45	1.25	1.03	0.25
100	3.056	3.302	14.6	1.12	3.59	1.32	1.08	0.26
125	3.065	3.315	15.2	1.18	3.74	1.41	1.13	0.26
150	3.074	3.329	16.1	1.25	3.72	1.50	1.20	0.26

The topological state of quantum materials has drawn tremendous attention in recent years. It is also interesting to further examine the topological properties of these VB-group diborides such as  $\text{TaB}_2$  and  $\text{NbB}_2$  which have high  $T_c$ . From the experimental perspective, the angle-resolved photoemission spectroscopy (ARPES) represents a powerful tool in probing the electronic structures, superconductivity, and topological properties of materials [65]. Theoretically, the topology denoted by topological indices  $Z_2$  ( $v_0; v_1 v_2 v_3$ ) can be determined by the symmetry of Bloch functions at eight special time-reversal invariant points, including one strong topological index  $v_0$  and three weak indices  $v_1, v_2, v_3$  [47,48,66,67]. It is found that both  $\text{TaB}_2$  and  $\text{NbB}_2$  are characterized by weak  $Z_2$  indices (0;001). This is the same as  $\text{MgB}_2$ , whose topological surface states were observed in recent experiments [68]. Our result is consistent with a recent theoretical report [66].

To further check the topological status of VB-group diborides, we construct the TaB<sub>2</sub> and NbB<sub>2</sub> (001) surfaces [see Fig. 6(a)], and study their surface states using the Green's function approach [69,70]. Using the Green's function surface model [71], the work function ( $\Phi$ ) of TaB<sub>2</sub> and NbB<sub>2</sub> (001) surfaces are 6.21 and 6.30 eV, respectively. To compare with ARPES, the spectral function is determined as

$$A(E, \mathbf{k}_{\parallel}) = -\frac{1}{\pi} \text{Im}[\mathbf{G}_{\mathbf{k}_{\parallel}}(E)], \quad (8)$$

$$\mathbf{G}_{\mathbf{k}_{\parallel}}(E) = [E - \mathbf{H}_{\mathbf{k}_{\parallel}}^{\text{DFT}} - \Sigma_{\mathbf{k}_{\parallel}}(E)]^{-1}. \quad (9)$$

Here,  $\mathbf{k}_{\parallel} = (k_a, k_b)$  is the transverse  $k$ -vector,  $\mathbf{G}_{\mathbf{k}_{\parallel}}(E)$  is the retarded Green's function of the surface system,  $\mathbf{H}_{\mathbf{k}_{\parallel}}^{\text{DFT}}$  refers to the DFT Hamiltonian of the surface region and the screening layers, and  $\Sigma_{\mathbf{k}_{\parallel}}(E)$  is the self-energy of the semi-infinite bulk part.

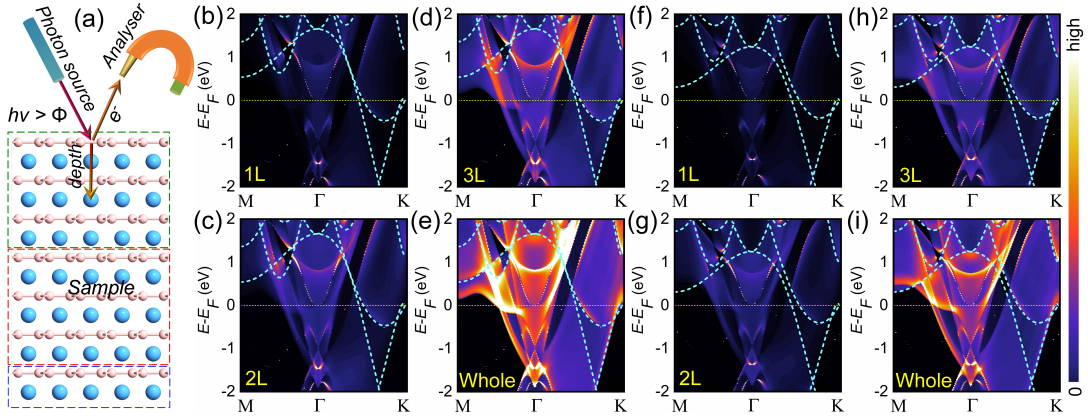


FIG. 6. (a) Schematic of detecting the electronic structures of MB<sub>2</sub> surface by ARPES set. The photon source energy  $h\nu$  should be larger than the work function  $\Phi$  of MB<sub>2</sub>. The blue, red, and green dot lines refer to the semi-infinite bulk, screening layers, and surface region of the used surface model, respectively. Spectral function with detection depths to the outermost monolayer (1L), the second layer (2L), the third layer (3L), as well as the whole slab structure (Whole). (b)-(e) for TaB<sub>2</sub> surface, (f)-(i) for NbB<sub>2</sub> surface. The sky-blue dot lines in (b)-(i) indicate the band structures of TaB<sub>2</sub> and NbB<sub>2</sub> bulk.

In ARPES measurements, the detector may display different features, depending on the probing depth. Figures 6(b)-6(e) give the spectral functions with detection depths to the outermost TaB<sub>2</sub> monolayer (labeled 1L), the second layer (2L), the third layer (3L), and the whole slab (Whole) of the TaB<sub>2</sub> (001) surface, respectively. We see that the 1L spectral function clearly illustrates the topological surface phase with a robust Dirac state near  $E_F$  around the  $\Gamma$  point. Its topological surface states become stronger when the detection depth increases. Figures 6(f)-6(i) illustrate the spectral functions of the NbB<sub>2</sub> (111) surface with different probing depths, where the same topological nature can be observed as TaB<sub>2</sub>. These results imply that both TaB<sub>2</sub> and NbB<sub>2</sub> have potential applications for integrating superconductivity and topological property in a single system.

#### IV. CONCLUSION

In conclusion, we have investigated the superconductivities and topological properties of several MgB<sub>2</sub>-type vdW layered structures using different exchange-correlation functionals. Density functional theory for superconductors can accurately reproduce  $T_c$  of MgB<sub>2</sub> when the OptB88-vdW functional is adopted. The spin-fluctuation was found to play a significant role in the superconductivities of VB-group diborides. In addition, we found that their  $T_c$  can be further enhanced by applying reasonable stretch strains. This work explicitly draws attention to the following key factors when one simulates superconductivities of materials, i.e., the reliable geometry, proper exchange-correlation functional such as those with the vdW correction, and inclusion of key mechanisms, such as the spin-fluctuation for real materials. Moreover, we demonstrated that both TaB<sub>2</sub> and NbB<sub>2</sub> have a topological surface state, suggesting their potential utilizations as topological superconductors in quantum devices. The present work may stimulate further development for the prediction of superconductors, with or without the topological properties.

## ACKNOWLEDGEMENTS

Work in China was supported by the National Natural Science Foundation of China (Grants No. 11774079 and No. 61774059), the Scientific and Technological Innovation Program of Henan Province's Universities (Grant No. 20HASTIT026), the Natural Science Foundation of Henan Province (No. 202300410226), the Young Top-notch Talents Project of Henan Province (2021 year), the Natural Science Foundation of Henan Normal University (No. 2020PL15), the Henan Overseas Expertise Introduction Center for Discipline Innovation (No. CXJD2019005), and the HPCC of HNU. Work at the UC Irvine was supported by the U.S. DOE, Basic Energy Science (Grant No. DE-FG02-05ER46237). We thank JP Hu at IOP of CAS for helpful discussions.

- [1] J. Bardeen, L. N. Cooper, and J. R. Schrieffer, *Phys. Rev.* **108**, 1175 (1957).
- [2] G. M. Eliashberg, *J. Exp. Theor. Phys.* **38**, 966 (1960).
- [3] A. B. Migdal, *J. Exp. Theor. Phys.* **34**, 1438 (1958).
- [4] E. R. Margine and F. Giustino, *Phys. Rev. B* **87**, 024505 (2013).
- [5] C.-S. Lian, C. Si, and W. Duan, *Nano Lett.* **18**, 2924 (2018).
- [6] Y. Zhao, C. Lian, S. Zeng, Z. Dai, S. Meng, and J. Ni, *Phys. Rev. B* **101**, 104507 (2020).
- [7] L. Yan, P.-F. Liu, H. Li, Y. Tang, J. He, X. Huang, B.-T. Wang, and L. Zhou, *npj Comput. Mater.* **6**, 94 (2020).
- [8] P. Morel and P. W. Anderson, *Phys. Rev.* **125**, 1263 (1962).
- [9] W. L. McMillan, *Phys. Rev.* **167**, 331 (1968).
- [10] R. C. Dynes, *Solid State Commun.* **10**, 615 (1972).
- [11] P. B. Allen and R. C. Dynes, *Phys. Rev. B* **12**, 905 (1975).
- [12] J. A. Flores-Livas, L. Boeri, A. Sanna, G. Profeta, R. Arita, and M. Eremets, *Phys. Rep.*

**856**, 1 (2020).

- [13]L. N. Oliveira, E. K. U. Gross, and W. Kohn, Phys. Rev. Lett. **60**, 2430 (1988).
- [14]M. Lüders, M. A. L. Marques, N. N. Lathiotakis, A. Floris, G. Profeta, L. Fast, A. Continenza, S. Massidda, and E. K. U. Gross, Phys. Rev. B **72**, 024545 (2005).
- [15]M. A. L. Marques, M. Lüders, N. N. Lathiotakis, G. Profeta, A. Floris, L. Fast, A. Continenza, E. K. U. Gross, and S. Massidda, Phys. Rev. B **72**, 024546 (2005).
- [16]J. A. Flores-Livas and A. Sanna, Phys. Rev. B **91**, 054508 (2015).
- [17]M. Kawamura, R. Akashi, and S. Tsuneyuki, Phys. Rev. B **95**, 054506 (2017).
- [18]A. Sanna, C. Pellegrini, and E. K. U. Gross, Phys. Rev. Lett. **125**, 057001 (2020).
- [19]M. Kawamura, Y. Hizume, and T. Ozaki, Phys. Rev. B **101**, 134511 (2020).
- [20]J. A. Flores-Livas, A. Sanna, and E. K. U. Gross, Eur. Phys. J. B **89**, 63 (2016).
- [21]R. Akashi and R. Arita, Phys. Rev. Lett. **111**, 057006 (2013).
- [22]F. Essenberg, A. Sanna, A. Linscheid, F. Tandetzky, G. Profeta, P. Cudazzo, and E. K. U. Gross, Phys. Rev. B **90**, 214504 (2014).
- [23]T. Nomoto, M. Kawamura, T. Koretsune, R. Arita, T. Machida, T. Hanaguri, M. Kriener, Y. Taguchi, and Y. Tokura, Phys. Rev. B **101**, 014505 (2020).
- [24]A. Floris, A. Sanna, M. Lüders, G. Profeta, N.N. Lathiotakis, M.A.L. Marques, *et al.*, Physica C **456**, 45 (2007).
- [25]J. P. Perdew, K. Burke, and M. Ernzerhof, Phys. Rev. Lett. **77**, 3865 (1996).
- [26]D. Vanderbilt, Phys. Rev. B **41**, 7892 (1990).
- [27]J. Nagamatsu, N. Nakagawa, T. Muranaka, Y. Zenitani, and J. Akimitsu, Nature **410**, 63 (2001).
- [28]J. P. Perdew, J. A. Chevary, S. H. Vosko, K. A. Jackson, M. R. Pederson, D. J. Singh, and C. Fiolhais, Phys. Rev. B **46**, 6671 (1992).
- [29]Y. Zhang and W. Yang, Phys. Rev. Lett. **80**, 890 (1998).
- [30]J. P. Perdew, A. Ruzsinszky, G. I. Csonka, O. A. Vydrov, G. E. Scuseria, L. A. Constantin, X. Zhou, and K. Burke, Phys. Rev. Lett. **100**, 136406 (2008).
- [31]J. Klimeš, D. R. Bowler, and A. Michaelides, J. Phys.: Condens. Matter **22**, 022201 (2010).
- [32]T. Thonhauser, S. Zuluaga, C. A. Arter, K. Berland, E. Schröder, and P. Hyldgaard, Phys.

Rev. Lett. **115**, 136402 (2015).

[33] T. Thonhauser, V. R. Cooper, S. Li, A. Puzder, P. Hyldgaard, and D. C. Langreth, Phys. Rev. B **76**, 125112 (2007).

[34] K. Choudhary, G. Cheon, E. Reed, and F. Tavazza, Phys. Rev. B **98**, 014107 (2018).

[35] K. Choudhary, K. F. Garrity, A. C. E. Reid, B. DeCost, A. J. Biacchi, A. R. Hight Walker, *et al.*, npj Comput. Mater. **6**, 173 (2020).

[36] P. Giannozzi, O. Andreussi, T. Brumme, O. Bunau, M. Buongiorno Nardelli, M. Calandra, *et al.*, J. Phys.: Condens. Matter **29**, 465901 (2017).

[37] D. R. Hamann, Phys. Rev. B **88**, 085117 (2013).

[38] M. Schlipf and F. Gygi, Comput. Phys. Commun. **196**, 36 (2015).

[39] G. Prandini, A. Marrazzo, I. E. Castelli, N. Mounet, and N. Marzari, npj Comput. Mater. **4**, 72 (2018).

[40] M. Kawamura, Y. Gohda, and S. Tsuneyuki, Phys. Rev. B **89**, 094515 (2014).

[41] S. Baroni, S. de Gironcoli, A. Dal Corso, and P. Giannozzi, Rev. Mod. Phys. **73**, 515 (2001).

[42] <http://sctk.osdn.jp/>.

[43] J. Taylor, H. Guo, and J. Wang, Phys. Rev. B **63**, 121104(R) (2001).

[44] M. Brandbyge, J.-L. Mozos, P. Ordejón, J. Taylor, and K. Stokbro, Phys. Rev. B **65**, 165401 (2002).

[45] J. M. Soler, E. Artacho, J. D. Gale, A. García, J. Junquera, P. Ordejón, and D. Sánchez-Portal, J. Phys.: Condens. Matter **14**, 2745 (2002).

[46] S. Grimme, J. Comput. Chem. **27**, 1787 (2006).

[47] L. Fu and C. L. Kane, Phys. Rev. B **76**, 045302 (2007).

[48] L. Fu, C. L. Kane, and E. J. Mele, Phys. Rev. Lett. **98**, 106803 (2007).

[49] H. J. Choi, D. Roundy, H. Sun, M. L. Cohen, and S. G. Louie, Nature **418**, 758 (2002).

[50] A. Floris, G. Profeta, N. N. Lathiotakis, M. Lüders, M. A. L. Marques, C. Franchini, E. K. U. Gross, A. Continenza, and S. Massidda, Phys. Rev. Lett. **94**, 037004 (2005).

[51] D. Yuan, Y. Zhang, W. Ho, and R. Wu, J. Phys. Chem. C **124**, 16926 (2020).

[52] See Supplemental Material at <http://link.aps.org/supplemental/XXX> for more details of partial results, which includes Refs. [11, 27, 47, 48, 55–57].

- [53] A. Shukla, M. Calandra, M. d'Astuto, M. Lazzeri, F. Mauri, C. Bellin, *et al.*, Phys. Rev. Lett. **90**, 095506 (2003).
- [54] M. Kawamura, Comput. Phys. Commun. **239**, 197 (2019).
- [55] I. Errea, F. Belli, L. Monacelli, A. Sanna, T. Koretsune, T. Tadano, *et al.*, Nature **578**, 66 (2020).
- [56] X.-M. Zhao, K. Zhang, Z.-Y. Cao, Z.-W. Zhao, V. V. Struzhkin, A. F. Goncharov, *et al.*, Phys. Rev. B **101**, 134506 (2020).
- [57] X. Zhang, M. Zhao, and F. Liu, Phys. Rev. B **100**, 104527 (2019).
- [58] J.-J. Zheng and E. R. Margine, Phys. Rev. B **94**, 064509 (2016).
- [59] Y. Cao, V. Fatemi, S. Fang, K. Watanabe, T. Taniguchi, E. Kaxiras, and P. Jarillo-Herrero, Nature **556**, 43 (2018).
- [60] P. Wang, R. Kumar, E. M. Sankaran, X. Qi, X. Zhang, D. Popov, *et al.*, Inorg. Chem. **57**, 1096 (2018).
- [61] J. E. Schirber, D. L. Overmyer, B. Morosin, E. L. Venturini, R. Baughman, D. Emin, H. Klesnar, and T. Aselage, Phys. Rev. B **45**, 10787 (1992).
- [62] H. Kotegawa, K. Ishida, Y. Kitaoka, T. Muranaka, N. Nakagawa, H. Takagiwa, and J. Akimitsu, Physica C **378-381**, 25 (2002).
- [63] D. Kaczorowski, A. J. Zaleski, O. J. Żogał, and K. Klamut, arXiv:cond-mat/0103571
- [64] H. Takeya, K. Togano, Y. S. Sung, T. Mochiku, and K. Hirata, Physica C **408-410**, 144 (2004).
- [65] C. Li, X. Wu, L. Wang, D. Liu, Y. Cai, Y. Wang, *et al.*, Phys. Rev. X **10**, 031033 (2020).
- [66] K.-H. Jin, H. Huang, J.-W. Mei, Z. Liu, L.-K. Lim, and F. Liu, npj Comput. Mater. **5**, 57 (2019).
- [67] Y. Zhou, B. Li, Z. Lou, H. Chen, Q. Chen, B. Xu, *et al.*, Sci. China Phys. Mech. Astron. **64**, 247411 (2021).
- [68] X. Zhou, K. N. Gordon, K.-H. Jin, H. Li, D. Narayan, H. Zhao, *et al.*, Phys. Rev. B **100**, 184511 (2019).
- [69] J. M. Marmolejo-Tejada, K. Dolui, P. Lazić, P.-H. Chang, S. Smidstrup, D. Stradi, K. Stokbro, and B. K. Nikolić, Nano Lett. **17**, 5626 (2017).
- [70] S. Smidstrup, D. Stradi, J. Wellendorff, P. A. Khomyakov, U. G. Vej-Hansen, M.-E. Lee,

*et al.*, Phys. Rev. B **96**, 195309 (2017).

[71] Y. An, Y. Hou, S. Gong, R. Wu, C. Zhao, T. Wang, Z. Jiao, H. Wang, and W. Liu, Phys. Rev. B **101**, 075416 (2020).